Forestry *An Internal Journal of Forest Research*

Institute of Chartered Foresters

Transverse fracture properties of green wood and the anatomy of six temperate tree species

Seray Özden[1*], Anthony Roland Ennos[2] and Marco E. G. V. Cattaneo[3]

[1]*Faculty of Life Sciences, University of Manchester, Manchester, M13 9PT, UK*

[2]*School of Biological, Biomedical and Environmental Sciences, University of Hull, Hull, HU6 7RX, UK*

[3]*Department of Mathematics, University of Hull, Hull, HU6 7RX, UK*

*Corresponding author: Email: seray.ozden@manchester.ac.uk

The aim of this study was to investigate the effect of wood anatomy and density on the mechanics of fracture when wood is split in the radial–longitudinal (RL) and tangential–longitudinal (TL) fracture systems. The specific fracture energies (G_f, Jm^{-2}) of the trunk wood of six tree species were studied in the green state using double-edge notched tensile tests. The fracture surfaces were examined in both systems using Environmental Scanning Electron Microscopy (ESEM). Wood density and ray characteristics were also measured. The results showed that G_f in RL was greater than TL for five of the six species. In particular, the greatest degree of anisotropy was observed in *Quercus robur* L., and the lowest in *Larix decidua* Mill. ESEM micrographs of fractured specimens suggested reasons for the anisotropy and differences across tree species. In the RL system, fractures broke across rays, whose walls unwound like tracheids in longitudinal–tangential (LT) and longitudinal–radial (LR) failure, producing a rough fracture surface which would absorb energy, whereas in the TL system, fractures often ran alongside rays.

Introduction

The long organs of trees (e.g. trunks and branches) must withstand environmental stresses to survive in nature by combining flexibility and rigidity. They do this by laying down wood which provides excellent mechanical support (McMahon, 1973). Compared to other structural materials, wood is strong, stiff, and tough, while still being lightweight (Gibson and Ashby, 1988; Niklas, 1992). It has thus been extensively used by mankind for centuries as one of the most popular structural and building materials. However, the structure of wood is rather complex, since it is composed of a wide

variety of cells. Therefore, wood is often considered to be a cellular solid characterised by a high degree of anisotropy at all levels of the anatomical organisation (Figure 1a) (Panshin and de Zeeuw, 1980).

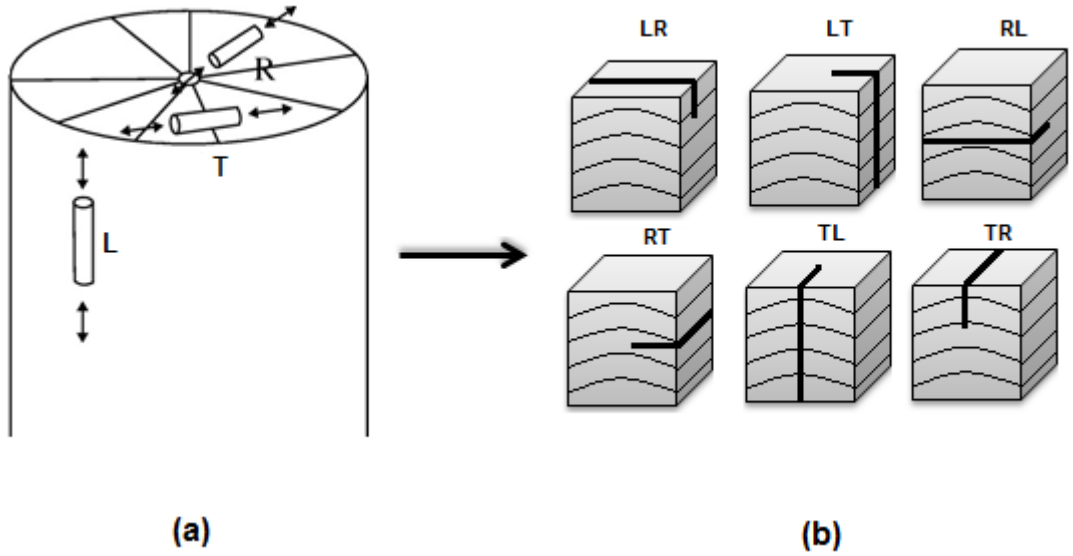

Figure 1 (a) Three main directions of wood (L is longitudinal, R is radial and T is tangential). Most of the wood cells are oriented longitudinally (tracheids/fibres and vessels), while rays in which the cells are oriented radially. As a consequence mechanical tests on oriented samples show that tangentially (T) wood is weaker than radially (R) and much weaker than longitudinally (L). Wood is readily split or crushed along the centre-line along which the rays and tracheids provide no reinforcement (Ennos and van Casteren, 2010). **(b)** A schematic illustration of six crack propagation systems.

Due to differences in wood anatomy, its properties can not only vary considerably between conifer and hardwood trees but also show differences within and among trees of the same species. The main structure of conifers comprises tracheids (around 90–95%), which are longitudinally oriented and provide both water conduction and structural support (Thomas, 2000; Ennos, 2001; Bowyer *et al.*, 2003). Conifer wood also contains radially orientated parenchyma cells, (arranged in thin vertical rows called rays); some conifers also have a small number of transversely oriented ray tracheids. In contrast, hardwoods have a relatively heterogeneous structure because the wood is composed of several different cell types, primarily fibres, vessels and rays. The longitudinally oriented fibres provide mechanical strength (Gartner *et al.*, 1990) and make up around 50% of the wood volume. In contrast, vessels, which are also oriented longitudinally, perform most of the water conduction and make up roughly 30% of the wood volume. Hardwoods further have radially oriented rays, which serve primarily two functions: providing radial reinforcement, and storing water and food and transporting them through wood (Barnett and Jeronimidis, 2003). There are marked differences in the size and proportion of rays between conifers and hardwoods. In conifers, rays tend to form a smaller proportion of wood volume (around 5–10%), and conifers usually have uniseriate rays (one cell wide). In contrast, hardwood rays constitute a far greater volume of wood structure (around 10–32%), and rays can be either uniseriate (one cell wide) or multiseriate (more than two cells wide), usually wider and longer than those of conifers (Clarke, 1933; Haygreen and Bowyer, 1982; Carlquist, 1988; Desch and Dindwoodie, 1996; Persson, 2000; Reiterer *et al.*, 2002; Bowyer *et al.*, 2003; Gibson, 2005; van Casteren et al., 2012). However, there are no tangentially oriented cells in either conifers or hardwoods.

Because of its anatomical complexity, it is quite difficult to measure the toughness of wood, as several factors affect it: the direction of the development of cracks, the anatomy, and the density of tree species (Nairn, 2007; Coureau *et al.*, 2013). Toughness is one of the most important fracture properties of wood that predicts how it fails and splits (its fracture mechanism). It is defined as the

ability of a material to absorb energy before complete fracture occurs. The fracture properties of wood differ in the three main orthotropic directions: longitudinal (L), radial (R) and tangential (T), and in the six possible fracture systems: LR, LT, RL, RT, TL and TR (Figures 1a and b). In each fracture system (e.g. TR), the first letter refers to the direction of loading (e.g. "T" is for the tangential direction, normal to the fracture plane) and the second letter ("R" is for radial direction) is the direction of crack propagation. Wood can be relatively difficult or easy to split depending on the loading direction. It has been well established in previous studies that wood is much stronger and tougher longitudinally (across the grain, in the LR–LT fracture systems) than radially and tangentially (along the grain, in the RL–RT–TL–TR fracture systems) (Schniewind and Centeno, 1973; Jeronimidis, 1980; Ashby *et al.*, 1985; Reiterer *et al.*, 2002; Bowyer *et al.*, 2003; Ennos and van Casteren, 2010; van Casteren *et al.*, 2012). This is because most wood cells (particularly, fibres and tracheids) are oriented longitudinally and provide more structural strength in this direction (Dinwoodie, 1981; Desch and Dinwoodie, 1996; Thomas, 2000; Ennos, 2001; Bowyer *et al.*, 2003). In the case of the fracture mechanism of wood, previous studies have also reported that wood is extremely tough when cut across the grain because this absorbs huge amounts of energy as the cell walls buckle and the cellulose fibres unwind (Jeronimidis, 1980) to give a rough fracture surface. In contrast, splitting wood along the grain (transversely) is relatively easy because this largely involves separating the longitudinal tracheids, using much less energy and producing a smoother fracture surface. Therefore, much research has concentrated on testing wood along the grain: RL, RT, TL and TR. These are the commonly most used crack propagation systems described in the scientific literature, due to difficulties in carrying out toughness tests across the grain (LR and LT) (Johnson, 1973; Schniewind and Centeno, 1973; Stanzl-Tschegg *et al.*, 1995; Fruhmann *et al.*, 2002; Reiterer *et al.*, 2002a, 2002b; Nairn, 2007; de Moura *et al.*, 2008; Matsumoto and Nairn, 2012). However, between radial and tangential directions, it is less clear which direction is better and why. In most cases, wood is 30–50% stronger and tougher radially than tangentially (Reiterer *et al.*, 2002; Bowyer *et al.*, 2003; Ennos and van Casteren, 2010; van Casteren *et al.*, 2012). The directionality of properties between radial and tangential directions, known as transverse anisotropy, can primarily be explained by the orientation and structure of rays (Price, 1929; Easterling *et al.*, 1982; Gibson and Ashby, 1988; Burgert *et al.*, 2001; Reiterer *et al.*, 2002; Ennos and van Casteren, 2010; van Casteren *et al.*, 2012), tracheid geometry and wood density (Price, 1929; Boutelje, 1962; Kahle and Woodhouse, 1994; Thomas, 2000; Watanabe *et al.*, 2002; Moden and Berglund, 2008).

Previous studies have suggested different reasons for transverse anisotropy in conifers and hardwoods. In conifers, the anisotropy is mainly explained by tracheid geometry and wood density (Boutelje, 1962). In hardwoods, however, high radial mechanical properties were found to be more likely due to the existence of rays, because hardwoods contain a greater percentage of rays, which provide extra reinforcement to wood radially (Gibson and Ashby, 1988).

In general, most wood properties are influenced by wood density, such that increase in density makes wood tougher, stronger, and stiffer (Ifju and Kennedy, 1962; Petterson and Bodig, 1983; Ashby *et al.,* 1985; Smith and Chui, 1994), since denser woods have a larger amount of cell wall material per unit area. The difference in density is closely related to the proportion of latewood and earlywood, because latewood is usually the denser region of a growth ring, containing smaller diameter cells with thicker walls (and hence a small void volume with more solid cell wall material). However, earlywood is less dense and has large diameter cells with thinner walls (Gibson and Ashby, 1988; Barnett and Jeronimidis, 2003). The thick cell walls thus reinforce wood much more to resist loading stresses. There is also a large difference in density between conifers and hardwoods: hardwoods are often denser than conifers (Barnett and Jeronimidis, 2003).

Wood properties also show differences between dry and green conditions. Green wood is described as fresh cut wood that has never been dried out, and whose cell walls are fully saturated, so that they have a moisture content (MC) of around 30% to more than 200%, depending on tree species and environmental conditions (Simpson and Anton, 1999); this compares to around 12% MC in the air-dried state. It is known that the properties of green wood are quite different from those of

dry wood; the strength and stiffness properties of the former are generally much lower than the latter (particularly the modulus of rupture and modulus of elasticity). Green wood is also commonly less stiff across the grain than along it (Porter, 1964; Logemann and Schelling, 1992; Smith and Chui, 1994; Kretschmann and Green, 1996; Vasic and Stanzl-Tschegg, 2007). However, a review of the literature on the transverse properties of green wood shows relatively little work (Bodig and Jayne, 1982). Van Casteren *et al.* (2012) studied the breaking stress of green wood in three hardwoods in the longitudinal, radial, and tangential directions. Though the transverse strength was much lower than the longitudinal strength, there were also differences between tangential and radial strength; radial tensile strength was higher than tangential. A recent study by Ozden and Ennos (2014) also examined the fracture properties of green wood in three species of hardwood in the RT and TR fracture systems. Their results found green wood to be 50% tougher in the RT fracture system than the TR system. They suggested that transverse anisotropy might have occurred due to the rays, which could reinforce and toughen green wood much more in the RT fracture system, just as they do in dry wood (Reiterer *et al.*, 2002).

To date, several properties of stemwood have been extensively studied in different tree species, loading directions and environmental conditions (dry or green) to better understand the complex biomechanical structure and mechanism of wood. However, detailed knowledge of the fracture mechanism of green wood is still lacking, and it has rarely been studied along the grain (RL vs. TL) in different tree species.

The aim of this study was to investigate the relationship between the toughness (as quantified by specific fracture energy, expressed G_f, Jm^{-2}) and anatomical structure of trees in the green state, particularly considering the influence of ray characteristics and density on the mechanism of failure between six different tree species: *Quercus robur* L. (English oak), *Fraxinus excelsior* L. (European ash), *Prunus avium* L. (Wild cherry), *Larix decidua* Mill. (European larch), *Thuja plicata* Donn ex. D. Don (Western red cedar), and *Pinus sylvestris* L. (Scots pine). The G_f was measured both in the RL and TL fracture systems using double-edge notch tensile tests, and the fracture surfaces were analysed using ESEM for each tree species.

Material and methods

Plant materials

In this study, six tree species were chosen for a range of anatomy: *Quercus robur* L. and *Fraxinus excelsior* L., which are ring-porous hardwoods with a high proportion of rays; *Prunus avium* L., which is a diffuse-porous hardwood with few rays; and three conifers: *Larix decidua* Mill., *Thuja plicata* Donn ex. D. Don, and *Pinus sylvestris* L., all of which have very small rays. Each sample tree was selected at random – half the sample comprised hardwoods (*Q. robur*, *F. excelsior* and *P. avium*) and the other half conifers (*L. decidua*, *T. plicata* and *P. sylvestris*) – in order to determine the variation in specific fracture energies (G_f, Jm^{-2}) across the tree species. All six logs were harvested from live trees in the University of Manchester's arboretum at Jodrell Bank, Manchester, UK. The identification of each tree was independently verified to ensure the species description was correct.

Sampling and toughness testing

All samples came from six trees (for example, ash samples were sawn from the same tree of *F. excelsior*); thus, there was one sample tree per species. The logs were sawn at height of 1–1.5 m up the trunk from each of the six trees. Each log had a diameter of around 20–30 cm, and the logs varied in age from 25 to 40 years. They were placed separately into plastic bags and stored in a cold room at 3–4 °C so that they were kept hydrated and in a fresh condition at all times until tests were carried out. These sample logs were then sawn into two pieces on each side of the trees equally to obtain tangential and radial planes in such a way that tangential surfaces of each log were sawn parallel to the annual growth rings like flatsawn planks, in which growth rings produce a wavy

pattern. In contrast, radial surfaces of each log were cut radially like quartersawn planks, in which annual growth rings appear as straight lines (Figure 2).

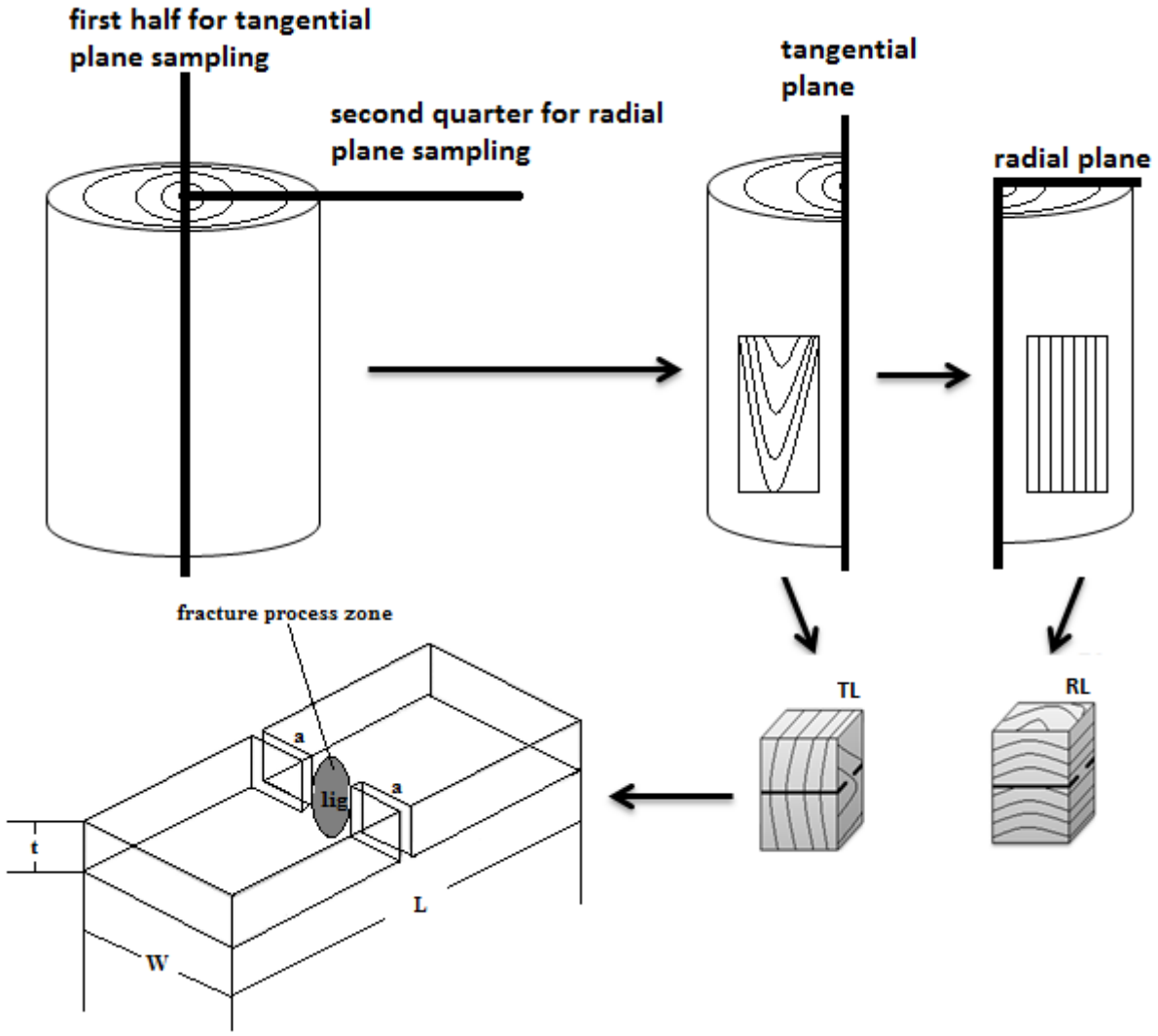

Figure 2 Illustration of sample preparation from radial (quartersawn) and tangential (flatsawn) planes to form RL and TL double-edge notched test specimens (where *L* is length, *w* is width, *t* is thickness, *a* is starter crack and *lig* is ligament length).

From each of the logs, five sample discs of 15 mm thickness were sawn both radially and tangentially. For the preparation of fracture test specimens, cuboids of wood were excised from these radial and tangential discs of each log having dimensions of 60 (length) x 15 (width) x 15 (thickness) mm^3 to form double-edge notched specimens, using a fret saw. For each disc, 8–10 cuboids of wood were cut halfway between the pith and bark. RL cuboids had the longest axis oriented radially and the shortest axis tangentially; TL cuboids had the long axis oriented tangentially and the shortest axis radially. This allowed us to determine how cuboids of wood, cut in two directions, show differences in toughness and anatomical properties. All cuboids contained both earlywood and latewood parts of a growth ring together and did not have any knots, reaction wood, or decay. Consequently, for each six log, 60 small cuboids of wood were taken from sample discs: 30 cuboids of wood were RL-oriented and 30 cuboids of wood were TL-oriented. Therefore, altogether 360 cuboids of wood were sampled.

Tensile tests and load-displacement curves

Prior to testing, wood samples were immersed in water for 24 hours in an airtight container, thus keeping the wood fully hydrated (100% humidity) until testing, to avoid shrinkage microcracks. The next day, starter cracks around 2 mm long were cut from either side halfway along the specimens using a steel double-edge razor blade (0.11 mm thick), to obtain a ligament length around 5 mm long.

The specimens were then subjected to a tensile test using a Universal Testing Machine (INSTRON® model 4301) equipped with a 1 kN load cell and attached to an interfacing computer. The specimen was clamped between the jaw faces manually, gripped from above and below, with a gap of 25 mm between the upper and lower jaws. The specimen was then stretched at a crosshead speed of 3 mm min^{-1} until it failed. The displacement was measured using the machine crosshead motion. The jaw set contained pyramid serrated faced clamping surfaces, which held the specimen firmly and provided high enough gripping forces to prevent sliding between the specimen and clamps. The gripping force and the zero point were also checked before testing the specimen to prevent slippage.

The computer simultaneously plotted and recorded a curve of the load versus the displacement of the crosshead, so that the displacement output recorded by the system was actually the sum of the system compliance and the specimen deformation. Finally, the toughness properties of each specimen were quantified using the G_f equation. This is the total work, W_F (total dissipated energy, Joule), under the load-displacement curve needed to completely separate a specimen into two pieces per unit ligament area (A_{lig}, m^{-2}) (Equation 1):

$$G_f = \frac{W_F}{A_{lig}} \quad (1)$$

Density measurements

After the experiments, tested samples were kept at 4 °C in sealed plastic bags in a cold room. To measure density, wood specimens were immersed in water. In order to ensure the specimens were fully hydrated, they were weighed at 6-hour intervals over a period of 1–2 days until the mass was constant. Each specimen was then submerged in a beaker of water placed on top of an electronic balance. The increase in weight was divided by the density of water to obtain the volume of the wood sample (cm^3) (Archimedes' principle, Hacke *et al.*, 2000). Thereafter, the samples were kept in an oven at 65–70 °C for 2–3 days until dry, following which they were weighed. To calculate the density of wood, oven dry weight (0% MC) was divided by the "saturated" volume.

Anatomy and microscopic analysis (ESEM)

The fracture surfaces of the wood samples were examined using ESEM. Five specimens were chosen from each species to observe the fracture behaviour of the cells under each fracture system. The test samples were dried and coated with gold before the ESEM analysis. Each tree species and fracture system was investigated under a range of magnifications and resolutions using a 15 kV acceleration voltage in a Philips XL30 ESEM-FG series scanner.

To determine ray parameters (e.g. size, number and shape of rays, ray area and area fraction of rays), the specimens were prepared on the RL fracture systems. For each species, every sixth sample of tensile toughness tests was investigated. Therefore, a total of 30 samples were prepared for image analysis – five samples per tree species. The fracture surfaces of each sample were then photographed using a Leica MZ95 stereo microscope equipped with Leica Application Suite (LAS) Computer Image Analysis Software. The image analysis of each of the samples produced clear photographs, which were used for the investigation of ray characteristics and ray size measurements. Using these photographs, the ray numbers per unit area (mm^2) were counted using

the count tool. Then, the width (w) was measured perpendicular to the ray axis at the widest part of each ray using a vector line tool, and the height (h) of each ray was measured parallel to the ray axis again using the same tool, by dragging a vector line from the bottom of the ray row to its top. Thereafter, we calculated all individual ray areas per unit area (mm^2) for each of the five samples per tree species by using the area equation for an ellipse (Equation 2), on the assumption that rays have an elliptical shape. We then added up the all individual ray areas per sample to find the total area of rays per unit area. To determine the area fraction of the rays (%) per unit area (mm^2), finally, total ray numbers per unit area were multiplied by the total area of rays per unit area, and then average percentage of rays was taken.

$$Area\ of\ ray = \frac{\pi}{4} \times h \times w \tag{2}$$

Statistical method and analysis

Statistical analysis was carried out to determine whether the fracture system, wood density, and ray properties had a significant effect on the G_f. All statistical analyses were performed using the R statistical software package (R Core Team, 2015, version 3.1.3), with a 5 % significance level. In order to take into account the nested structure of the data, with all samples of a species coming from the same tree, a linear mixed-effects model was used. The dependence on the particular tree was modelled by a random effect, with no within-group correlations, since the original locations of the samples in each tree species were unknown. Fracture system (RL vs. TL) and wood densities were modelled as fixed effects: fracture system was a binary variable while wood density was a continuous variable. A logarithmic transformation of the response variable G_f was clearly suggested by its empirical distribution. Therefore, the natural logarithm of G_f was used as a response variable in the linear mixed-effects model, which was fitted using the method of restricted maximum likelihood. A variable selection based on Akaike's Information Criterion (AIC) excluded wood density and interaction terms (fracture system–density interaction) as redundant, reducing the model to one fixed effect: fracture system. According to the AIC criterion, the "best" model is the one with minimum AIC value.

Results

Tensile tests

A total of 360 samples were tested: 180 samples taken from each fracture system (RL vs. TL). The distribution of the mean G_f values and anisotropy across the six tree species and two fracture systems is detailed in Table 1. Tensile tests resulted in a clean fracture in both the RL and TL fracture systems, giving G_f values between 60 and 1000 Jm^{-2}.

It is notable in Table 1 that *Q. robur* had the highest mean G_f values, and *P. sylvestris* the lowest. Each tree species further showed different degrees of anisotropy (RL/TL) in their wood, the anisotropy varying from 1.2 to 2.2 (Table 1). In particular, *Q. robur* showed the greatest transverse anisotropy, its G_f being 2.2 times greater in the RL than in the TL fracture system (mean 1080 Jm^{-2} in RL and 488 Jm^{-2} in TL). *T. plicata* showed the second greatest anisotropy; G_f in the RL was almost 1.8 times greater than in the TL, with a mean G_f of 429 Jm^{-2} in RL and 239 Jm^{-2} in TL. However, the anisotropy factor was the least for *L. decidua*; G_f in RL was 1.2 times greater than G_f in TL, with means of 434 Jm^{-2} in RL and 361 Jm^{-2} in TL.

Table 2 shows the result of the average AIC values for fixed effect terms in all data. According to the AIC criterion, fracture system received the lowest AIC value and best represents the true relationship with the given data. While the density and interaction terms are redundant (Table 2). Therefore, a linear mixed-effects model was used to investigate the relationship of G_f and only the

fracture system as an explanatory factor across six tree species (Table 3). Both fixed (fracture system) and random effect (type of tree species) terms improved the mixed-effects model significantly (Table 3). The linear mixed-effects model presenting the dependence of the logarithm of G_f on the fracture system for all data is shown in Table 3. It can also be seen clearly that G_f was significantly affected by the fracture system ($p < 0.001$). According to the fitted model, G_f was 1.684 times larger on average when the fracture system was RL than when the fracture system was TL.

Table 1 Summary mean (±SE) specific fracture energies (G_f, Jm^{-2}) along the grain (RL vs. TL) and degree of anisotropy for six plant species obtained in tension tests.

	G_f (Jm^{-2})		Anisotropy
Species	**G_fRL**	**G_fTL**	**G_fRL/G_fTL**
Hardwoods			
Q. robur	1080.7±89.09 (n = 30)	488.1±36.61 (n = 30)	2.21
F. excelsior	643.8±82.55 (n = 30)	406.9±36.79 (n = 30)	1.58
P. avium	481.7 ±51.67 (n = 30)	351.7±42.65 (n = 30)	1.37
Conifers			
L. decidua	434.4±53.79 (n = 30)	361.2±37.23 (n = 30)	1.20
T. plicata	429.8±37.57 (n = 30)	239.8±21.72 (n = 30)	1.79
P. sylvestris	267.6±21.94 (n = 30)	187±19.20 (n = 30)	1.43

Table 2 Akaike's information criterion (AIC) for five fixed effect terms in all data (the number in bold means the minimum AIC that is selected as the best model).

Fixed Effect Terms	**AIC**
fracture system, density, interaction	605.40
fracture system, density	605.27
fracture system	**605.04**
density	656.17
(none)	656.00

Table 3 Linear mixed-effects model for six tree species, describing the effect of the fracture system on wood specific energies.

Fixed effects					
Parameter	**Value**	**Estimate (SE)**	**DF**	***t*-value**	***p*-value**
(Intercept)	6.093	0.167	353	36.494	0.000
fracture system (TL)	-0.443	0.056	353	-7.844	0.000
Random Effects					
Variance components	**StdDev**				
Intercept	0.397				
Residual	0.536				

A series of linear models were then developed for each species separately to determine the potential effects of wood density and fracture system on G_f values (Table 4). Each tree species showed different G_f values between RL and TL fracture systems. G_f was significantly greater in the RL fracture system than the TL fracture system in most species – *Q. robur* ($p < 0.001$), *F. excelsior* ($p < 0.001$), *P. avium* ($p < 0.05$), *T. plicata* ($p < 0.001$) and *P. sylvestris* ($p < 0.05$) – except in *L. decidua* ($p > 0.05$) (Table 4).

Table 4 Linear models for dependence of logarithm of specific fracture energy (G_f) on fracture system and density, for each tree separately. The interaction was not used between fracture system and density because the interaction term was not significant since it is the best one of 4 species: *Q. robur*, *F. excelsior*, *T. plicata* and *P. sylvestris*.

Fixed Effects for *Q. robur*				
Value		**Std.Error**	**t-value**	**p-value**
(Intercept)	4.828	1.371	3.52	0.001
fracture system (TL)	-0.861	0.129	-6.664	0.000
density	3.762	2.499	1.505	0.138
Fixed Effects for *F. excelsior*				
(Intercept)	10.867	2.514	4.322	0.000
fracture system (TL)	-0.559	0.158	-3.544	0.001
density	-8.464	4.664	-1.815	0.075
Fixed Effects for *P. avium*				
(Intercept)	4.981	1.361	3.659	0.001
fracture system (TL)	-0.297	0.135	-2.206	0.031
density	2.178	2.824	0.771	0.444
Fixed Effects for *L. decidua*				
(Intercept)	5.924	0.881	6.722	0.000
fracture system (TL)	-0.185	0.157	-1.176	0.245
density	-0.032	2.482	-0.013	0.990
Fixed Effects for *T. plicata*				
(Intercept)	7.363	0.867	8.496	0.000
fracture system (TL)	-0.720	0.151	-4.778	0.000
density	-4.266	2.602	-1.639	0.107
Fixed Effects for *P. sylvestris*				
(Intercept)	7.478	0.578	12.943	0.000
fracture system (TL)	-0.392	0.122	-3.204	0.002
density	-6.600	1.878	-3.514	0.001

In the case of density results, wood densities varied from 0.30 to 0.56 gcm^{-3} across six species. The greatest mean density values were obtained in *Q. robur* with a mean of 0.56 gcm^{-3}, followed by *F. excelsior*, *P. avium*, *L. decidua*, *T. plicata* and *P. sylvestris*, respectively. However, though the wood density was expected to explain higher G_f values across six species, there was no estimable relationship between G_f and density. According to AIC, the density was not as useful in the model as indicated by its higher AIC value (Table 2). . The results of linear models for the dependence of the logarithm of specific fracture energy (G_f) on density (Table 4) for each species separately showed that the effect of wood density was not significant on G_f values in most cases, except in *P. sylvestris*; surprisingly *P. sylvestris* indicated a significant negative relationship between G_f and wood density.

Load-displacement curves of each tree species

A total of 360 load-displacement curves were obtained from the tensile tests, and each curve was examined in detail to better understand the failure behaviour of each species and fracture systems. The double-edge notched tensile tests provided fairly distinct load-displacement curves within each tree species and fracture systems (RL vs. TL). Due to the large number of load-displacement curves from the tests, one typical example of each species and fracture system was shown in a diagram (Figure 3).

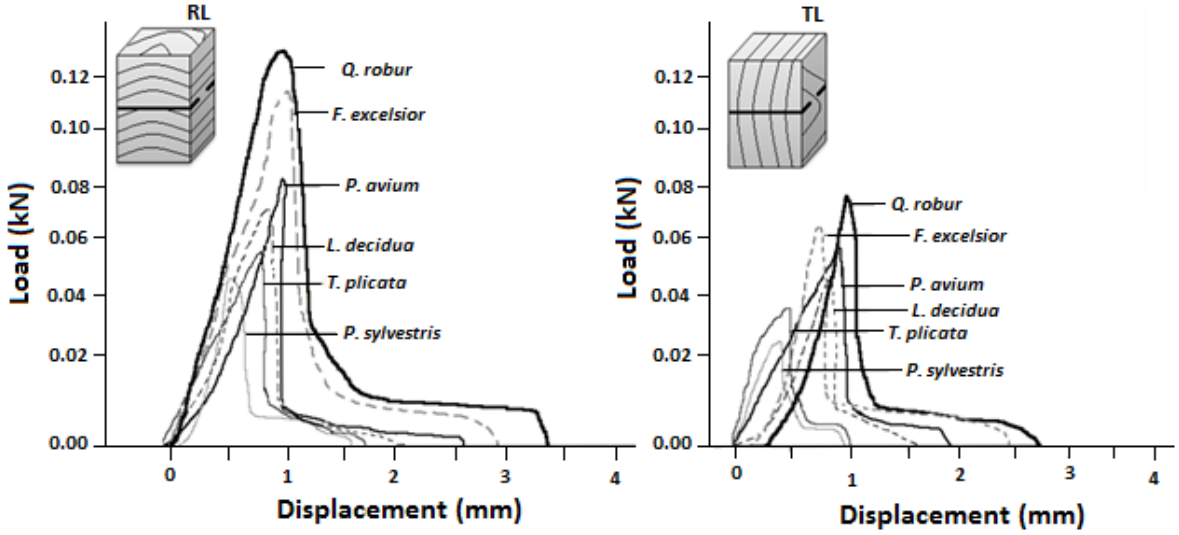

Figure 3 Load-displacement diagrams of tensile tests in the RL and TL fracture systems.

Therefore, representative "typical" load-displacement diagrams for each tree species are plotted in Figure 3 in both the RL and TL fracture systems. *Q. robur*, *F. excelsior* and *P. avium* all showed quite tough, ductile failure behaviour in their woods: the force rose quickly to fracture at significantly high loads, after which the load started to fall sharply. However, at still higher deflections, the load plateaued to some extent, with final failure only occurring at large deflections, particularly in the RL system (Figure 3). Consequently, the G_f was high. However, the conifers, *L. decidua*, *T. plicata* and *P. sylvestris* showed more semi-brittle or brittle failure behaviour in their woods: the initial slope and failure loads were much lower, and after peak loading, the force fell quite rapidly to zero. Therefore, though failure displacement was relatively high, the G_f was lower.

Maximum loads

However, between load-displacement curves in the RL and TL fracture systems, there were also differences in terms of the highest maximum load and fracture behaviour. The maximum loads varied from an average of 27 N to 100 N, with the highest loads observed in *Q. robur* with a value of 100 N and the lowest in *P. sylvestris*. Each species also had a higher maximum load on the RL fracture system than the TL system; *L. decidua* again showed the least anisotropy in its maximum loads.

According to the AIC criterion, fracture system–density interaction is the best model (Table 5). Therefore, we used a linear mixed-effects model for the dependence of maximum load on fracture system, density, and interaction for all data (Table 6). According to the linear mixed-effects model, only the interaction was significant among the fixed effects ($p < 0.05$), in such a way that wood density had a positive significant influence on maximum loads in the RL system, but a negative significant influence on maximum loads in the TL system (Table 6).

Table 5 Akaike's information criterion (AIC) for five fixed effect terms in all data (the number in bold means the minimum AIC that is selected as the best model).

Fixed Effect Terms	AIC
fracture system, density, interaction	**3172.4**
fracture system, density	3183.2
fracture system	3190.3
density	3251.4
(none)	3258.7

Table 6 Linear mixed-effects model for six tree species, describing the effect of the fracture system, density and fracture system-density interaction on maximum load.

Fixed effects					
Parameter	**Value**	**Estimate (SE)**	**DF**	***t*-value**	***p*-value**
(Intercept)	59.141	18.457	345	3.204	0.002
fracture system (TL)	0.293	9.312	345	0.031	0.975
density	17.431	39.240	345	0.444	0.657
interaction	-46.649	21.280	345	-2.192	0.029
Random Effects					
Variance components	**StdDev**				
Intercept	18.813				
Residual	21.225				

The measurements of the parameters of ray structure

Descriptive values of ray parameters are shown in Table 7. Each species showed clear differences in their ray dimensions and shape: *Q. robur* had both multiseriate and uniseriate rays; *F. excelsior* and *P. avium* had multiseriate rays; *L. decidua*, *T. plicata*, and *P. sylvestris* had uniseriate rays. The rays were more likely to have a homogeneous distribution in the structure of *F. excelsior*, which also showed greater values for total ray number, with a mean of 30.8 rays per mm^2. The mean percentage of rays was also the greatest in *Q. robur*, and lowest in *P. sylvestris*: *Q. robur* showed on average 24.4% rays per unit area (Table 7). *F. excelsior* had also on average 18.9% of rays per unit area. The mixed-effects model, however, was not conducted on ray parameters because five samples per tree species was not a large enough sample.

Discussion

The results of our tests showed very clear differences in G_f values across six tree species and two fracture systems. Our results confirm that G_f was mainly affected by the fracture system. Overall, the G_f was found to be, on average, almost 1.6 times greater in the RL system than in the TL system across six tree species. This agrees well with the results of earlier studies carried out on dry wood, which investigated both toughness and strength. Wood was found to be stronger and tougher in the RL system than the TL system (Stanzl-Tschegg *et al.*, 1995; Burgert *et al.*, 2001; Reiterer *et al.*, 2002; van Casteren *et al.*, 2012). The load-displacement diagrams and maximum loads also provided insights into the failure behaviour of each fracture system (Tschegg *et al.*, 2001). The RL fracture systems essentially showed a tough ductile failure behaviour, while TL fracture systems presented

more brittle failure behaviour. Our results reported that the maximum load in RL was, on average, 1.4 times greater than TL (Mean: 66.6±2.15 N in RL; 47.3±1.86 N in TL).

Table 7 Mean density (±SE) (n = 60 for each species) and ray measurement results (n = 5) for each species of six plant species. Ray results were obtained in only RL fracture system.

	Hardwoods			**Conifers**		
Anatomical Parameters	***Q. robur***	***F. excelsior***	***P. avium***	***L. decidua***	***T. plicata***	***P. sylvestris***
Density (gcm^{-3})	0.555±0.003	0.531±0.002	0.483±0.003	0.356±0.004	0.314±0.003	0.295±0.004
Ray Shape	Both multiseriate and uniseriate	multiseriate	multiseriate	uniseriate	uniseriate	uniseriate
Ray height (h) (mm)	0.71±0.098	0.39±0.013	0.38±0.006	0.29±0.001	0.25±0.007	0.24±0.009
Ray width (w) (mm)	0.085±0.013	0.057±0.003	0.055±0.004	0.028±0.001	0.029±0.003	0.027±0.001
h/w ratio (-)	8.47±0.665	6.9±0.388	6.97±0.509	10.43±0.792	8.66±0.244	9.18±1.010
Total ray number per unit area (mm^2)	23.6±4.004	30.8±8.952	21.8±1.392	13.8±1.593	12.8±1.067	11±1.449
Total ray area (mm^2)	1.04±0.347	0.50±0.079	0.36±0.046	0.08±0.015	0.07±0.005	0.05±0.008
Area fraction of rays per unit area (%)	24.42±9.196	18.99±8.495	8.06±1.469	1.35±0.344	0.87±0.135	0.68±0.159

Furthermore, each species had different degrees of anisotropy in their woods. Particularly, *Q. robur* showed the greatest anisotropy, its G_f being over twice as great in the RL than in the TL system, followed by *T. plicata*, *F. excelsior*, *P. sylvestris*, *P. avium*, and *L. decidua*. Our results agree with those of the study by Burgert *et al.* (2001), who also studied the mechanical properties of different tree species in the green state. Similarly, they found the radial modulus of *Q. robur* was, on average, 2.2 times greater than the tangential modulus; the radial modulus of *F. excelsior* was, on average, 1.6 times greater than the tangential modulus. A previous study by Boutelje (1962) reported that wood density was the main reason for transverse anisotropy in conifers. In our study, however, the wood densities did not vary significantly between RL and TL fracture systems of each tree species. Therefore, the G_f results of our study suggested that density may not have any influence on transverse anisotropy across the six species. However, further studies should be carried out on different tree species between RL and TL fracture systems to better understand the influence of density on G_f values.

We could explain the differences of the two fracture systems largely by considering both the presence of rays and cell shape, which in turn affected the mode of fracture. It is known that rays provide a mechanically strong structure that tends to resist crack propagation radially (Schniewind, 1959; Beery *et al.*, 1983; Ashby *et al.*, 1985; Mattheck and Kubler, 1995; Burgert *et al.*, 1999, 2001; Reiterer *et al.*, 2001, 2002a, 2002b). However, some authors suggested that rays act as either fracture initiators (longitudinally) or fracture arrestors (transversely) (Keith and Cote, 1968; Delorme

and Verhoff, 1976; Cote and Hanna, 1983; Mattheck and Breloer, 1994; Bodner *et al.*, 1997; Reiterer *et al.*, 2002).

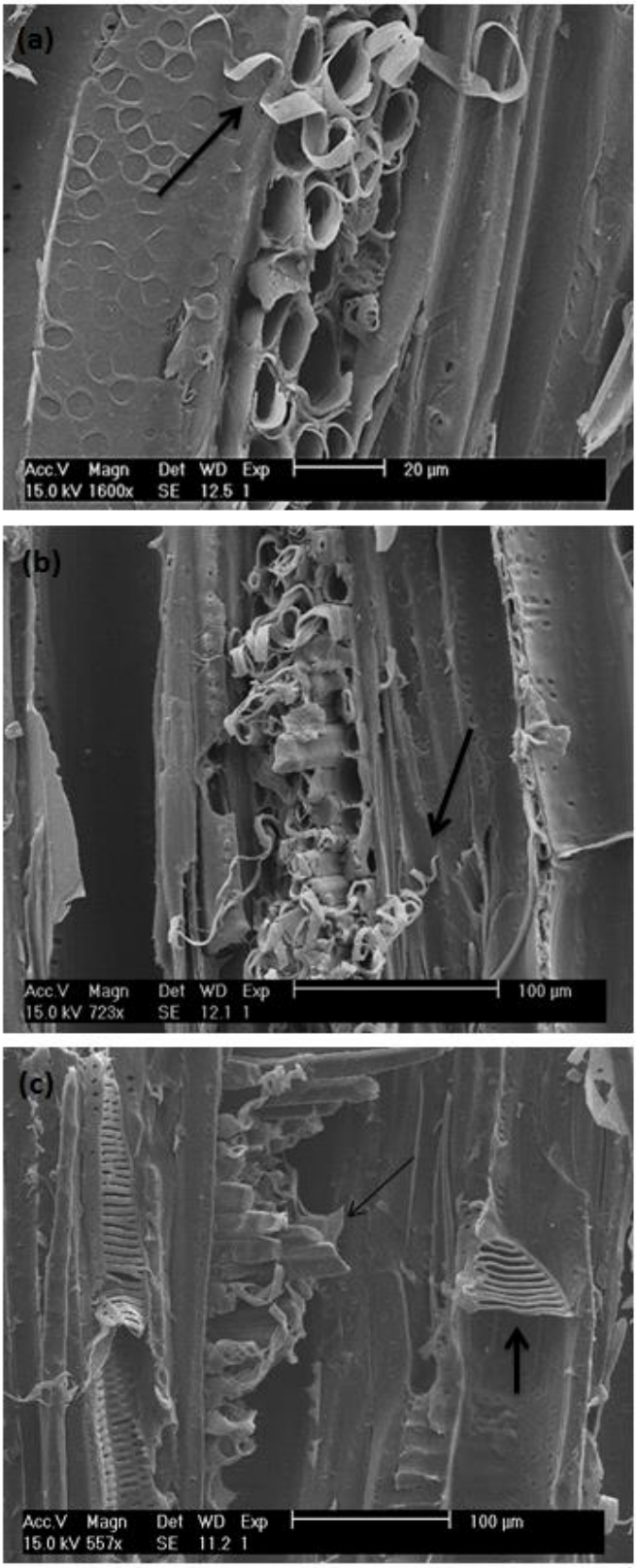

Figure 4 ESEM micrographs of hardwood fracture surfaces. **(a)** RL fracture surface of *P. avium*; arrow shows spiral failures of rays. **(b)** RL fracture surface of *Q. robur*; the arrow shows fracture mainly occurs in spiral manner through rays and rays have much thicker cell walls. **(c)** TL fracture surface of *Q. robur*; thin arrow indicates cross cell failure in rays and thick arrow shows cell rupture in vessels.

Our fracture surface analysis showed clear differences in the failure patterns between the RL and TL fracture systems for each species. The micrographs showed that when the fracture cut through rays in the RL system, the rays strongly resisted it. *Q. robur* had the highest G_f and the highest anisotropy between RL and TL, probably because it had the highest percentage of rays in the RL system (around 25%). Spiral and buckling failure was most common in *Q. robur* as well. Therefore, much more energy was used to break the rays, resulting in an apparently ductile failure (Figure 4b). Particularly in hardwoods, this involved spiral failure of the ray walls (Figure 4a, b). This rough structure could be also due to the unravelling of cellulose fibrils (microfibrils) in the walls, which is the same mechanism seen in tracheids and fibres (tension buckling mechanism) and which toughens wood across the grain (Gordon and Jeronimidis, 1974; Jeronimidis, 1980). This mechanism suggested to us that spiral failures could be related to the organisation of the fibril (microfibrillar) angle of the cell wall. According to Gordon and Jeronimidis (1980), when a crack starts to grow across the grain, all stresses diffuse around the crack tip, and thus, during tensile loading, fibres and tracheids split or buckle, producing independent thin tube-shaped helically wound cell walls. The unwinding of the helical fibres results in a large displacement, resulting in elongations of more than 20% before the wood is fractured completely (Page *et al.*, I97I; Hardacker and Brozinski, I973). Before the actual fracture occurs, therefore, a considerable amount of energy is needed, even though the force is relatively low due to the large elongation in the cells (Gordon and Jeronimidis, 1974; Jeronimidis, 1980). This is consistent with the high work of fracture found by Gordon and Jeronimidis (1980) in their model wood when reinforced with fibres set at a large angle to the axis of their model xylem cells (Gordon and Jeronimidis, 1980).

The cell geometries of each wood cell vary along wood axes, and this cell geometry could have a direct influence on the failure mechanism of wood. A previous study by Price (1929) used a honeycomb model to determine the elastic properties of wood in each direction because the cell geometry of wood cells is similar to the structure of a honeycomb. The tracheid honeycomb was estimated by “a close–packed array of circular tubes”. The cell wall requires an extension in order to stretch longitudinally, while an extension is not necessary in order to stretch wood in the radial and tangential directions. Deformation could simply be provided by bending the walls. This is different in the radial and tangential directions, since they have low macroscopic stiffness (Price, 1929; Gibson and Ashby, 1982; Kahle and Woodhouse, 1994). Similarly, transverse anisotropy could be explained by the shape and arrangement of rays in our study. In the RL system, rays are composed of radially elongated parenchyma cells, which are attached to each other like straight radial rows of ribs and are more likely to have a regular array of close-packed hexagonal cells. This type of arrangement and shape of cells could act as a strengthening function in the RL system, such that when the crack was initiated by stretching the specimen, tensile stresses were carried out from cell to cell in the aggregations of rays around the crack tip. Therefore, this process could minimise and lessen the speed of crack propagation (Reiterer *et al.*, 2002, Ozden and Ennos, 2014). During the crack growth in the RL fracture system, the presence of rays may also play a contributing role to fibre bridges, in that tensile stresses are advanced by rays from the fracture process zone (Beery *et al.*, 1983; Burgert *et al.*, 2001; Reiterer *et al.*, 2002a). Thus, the larger the percentage of rays, the greater the energy required to build up fibre-bridging zones to resist crack growth. Additionally, much larger displacements occur in cells along the RL system. After specimens separated into two pieces, the RL system showed rougher surfaces than the TL fracture system due to the extra mechanical support of ray cells in the RL system.

In contrast, in the TL fracture system, the longitudinal arrangement of rays could act as a fracture initiator for the crack path because rays were located along the same axis of applied load (Ashby *et al.*, 1985; Desch and Dinwoodie, 1996; Burgert *et al.*, 1999; Bowyer *et al.*, 2003). Thus, rays may weaken the surface contact between fibres and tracheids (Figures 4c, 5a) and will be easier to split from their neighbouring cells (Ozden and Ennos, 2014). As a result, cracks can grow more easily and less energy is needed to break the wood in the TL system. In between rays, fractures could also run through vessels, particularly in early wood because less energy was required to break through these

cells. The micrographs of *Q. robur* in the TL system showed cell wall fractures through the vessels, which also acted as fracture initiators, splitting and deforming easily by either transwall or intracellular failures than in the RL fracture (Figure 4c) (Ashby *et al.*, 1985; Desch and Dinwoodie, 1996; Burgert *et al.*, 1999; Reiterer *et al.*, 2002; Bowyer *et al.*, 2003). In the TL system, thus, the wood had a smoother and flatter fracture surface, in which fracture can be described as a peeling or clean failure.

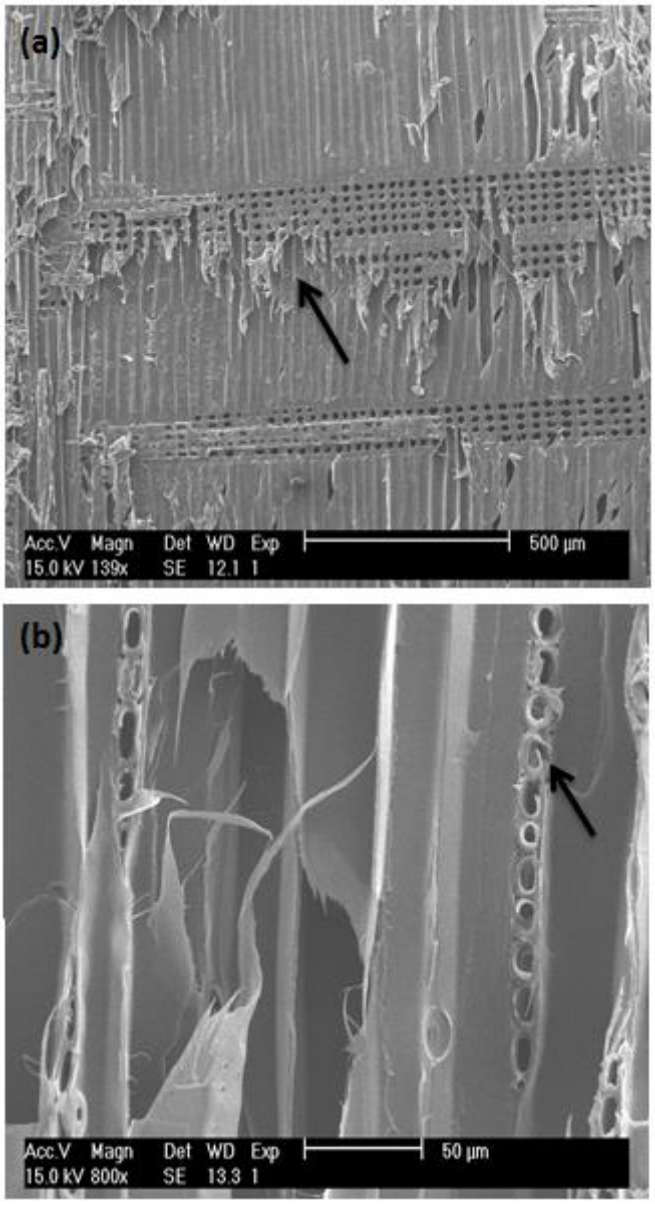

Figure 5 ESEM micrographs of conifers fracture surfaces. **(a)** TL fracture surface of *P. sylvstris*; crack deforms early wood tracheid cells and cells seem to have more intracellular cell deformations due to thin cell walls. **(b)** RL fracture surface of *T. plicata*; fracture is seen as mainly cell ruptures and rays have thin cell walls.

Similar to hardwoods, conifers also presented the same contrasting failure behaviour between RL and TL fracture systems, such that conifers tended to fail more easily in the TL system than the RL system. At the microscopic level, this anisotropy can be explained due to the manner of rays and tracheids cells during crack propagation. This is because the cracks travelled more between tracheids in the RL system by cell ruptures, and more energy was required to fail in the RL system in this phase (Figure 5b). However, on the TL fracture system, crack growth had two options, as cracks may encounter tracheids, which provide a slightly tough region, or they might find a shortcut to grow

rapidly alongside rays (Figure 5a). Therefore, the TL system showed more brittle failure events by cell separations.

However, relating to why G_f values showed considerable differences between hardwoods and conifers is still not completely explained. One reason might be based on the fact that the anatomy of hardwood and conifer is different. In particular, the misalignment of fibre may lead to a more tortuous crack path, and so, to a more energetic toughening mechanism in hardwoods compared to the relatively straight crack path observed in conifers, where tracheids are well aligned. On the other hand, our study showed that the anatomy of hardwoods was strengthened by a greater percentage of ray tissue; on average 16.5%, compared with only 1% in conifers. Therefore, the influence of rays in conifers could be negligible, but further analysis should be considered.

One aspect of our results was unexpected. The G_f values we found for *Q. robur* 480–1080 Jm^{-2} were more than twice that found in dry wood by Reiterer *et al.* (2002), who found G_f values of *Q. robur* ranged between 270–350 Jm^{-2} in the TL and RL systems, respectively. However, for *F. excelsior*, we found nearly the same results. Tukiainen and Koponen (2006) studied the fracture behaviour of green birch and spruce wood in the RT system, and they found higher values: $G_{f;}$ value for dry birch (12% MC) was 1623 Jm^{-2} and for wet birch (52% MC) was 985 Jm^{-2}. Vasic and Stanzl-Tschegg (2007) also studied the G_f of different species in the green state. At 98% relative humidity and green conditions, the G_f of *Quercus alba* was found to be 747 Jm^{-2} in the RL fracture system and 373 Jm^{-2} in the TR fracture system. The difference of G_f values of *Q. robur* could be because our methods were different from those authors (they used the wedge splitting Mode I fracture behaviour), and *Q. robur* could develop microcracks during drying more than *F. excelsior*, but this is not certain. However, there are no clear data in the literature to prove whether the G_f is moisture dependent or not (Larsen and Gustafsson, 1990; Rug *et al.*, 1990; Valentin *et al.*, 1991; Smith and Chui, 1994). Therefore, more research should be performed comparing fracture properties between green and dry wood using the same test technique and tree species.

Conclusion

In conclusion, we compared failure modes and G_f values in the RL and TL fracture systems of six tree species. We clearly showed that G_f values are mainly related to the fracture system. There was a great anisotropy between the two fracture systems; green wood had a higher G_f in the RL system than TL, such that splitting wood in the TL system was much easier than in the RL system, at least in the species we studied. ESEM micrographs also showed that in the RL system, cells failed mostly in intercellular or the intracellular failure manner in a more ductile fashion, while cracks propagated more easily as producing great cell deformations such as cell ruptures and breakings in transwall fracture by a brittle fashion in the TL fracture system. The helical pattern of cellulose microfibrils in the secondary wall was previously reported (Gordon and Jeronimidis, 1980). Here, we found quite a similar mechanism in the cell walls of ray cells in hardwoods, which failed mostly by helical or spiral failure fashion in the RL fracture system. We thus suggest that the fracture mechanism of rays, particularly in hardwoods, act like fibres or tracheids to reinforce wood in the RL system. However, conifers showed more cell deformations in both fracture systems compared to hardwoods. The cracks generated consistently straight cuts even across the rays. We could suggest that the high contribution of rays to the volume of hardwoods could strengthen their wood to the crack growths more than conifers, which showed a lower area fraction of rays. However, we do not have enough data to clearly determine why there was anisotropy between RL and TL fracture systems and why conifers split easily and have lower specific fracture energies. Therefore, more research is needed to better understand the effect of wood anatomy on the fracture properties. It would also be useful to study more tree species to determine the function of rays on the fracture properties.

Acknowledgements

We would like to thank Becky Burns of the Jodrell Bank Discovery Centre, University of Manchester, with help in collecting green wood trunks. Great thanks are also due to Dr John Waters and Jim Backhouse, University of Manchester, for helping us with the ESEM analysis and sample cutting. Professor Alexis Achim provided useful editorial comments and criticism that we gratefully acknowledge. We also would like to thank our anonymous reviewers for the great effort they have put into reviewing our paper.

References

Ashby, M.F., Easterling K.E., Harrysson, R. and Maiti, S.K. 1985 The fracture and toughness of woods. *Proc. Roy. Soc. Lond. A* **398**, 261 - 280.

Barnett, J. and Jeronimidis, G. 2003 *Wood quality and its biological basis*. In Blackwell, London, UK: Blackwell, 226 pp.

Beery, W.H., Ifju, G. and McLain, T.E. 1983 Quantitative wood anatomy-relating anatomy to transverse tensile strength. *Wood Fiber Sci.* **15**, 395 - 407.

Bodig, J. and Jayne, B.A. 1982 *Mechanics of wood and wood composites*. Van Nostrand Reinhold, New York, 712 pp.

Bodner, J., Schlag, M.G. and Grull, G. 1997 Fracture initiation and progress in wood specimens stressed in tension. Part I: Clear wood specimens stressed parallel to the grain. *Holzforschung* **51**, 479 - 484.

Boutelje, J.B. 1962 The relationship of structure to transverse anisotropy in wood with reference to shrinkage and elasticity. *Holzforschung* **16**, 33 - 46.

Bowyer, J.L., Shmulsky, R. and Haygreen, J.G. 2003 *Forest products and wood science: an introduction*. Iowa State Press, Iowa, 554 pp.

Burgert, I., Bernasconi, A. and Eckstein, D. 1999 Evidence for the strength function of rays in living trees. *Holz als Roh- und Werkstoff* **57**, 397 - 399.

Burgert, I., Bernasconi, A., Niklas, K.J. and Eckstein, D. 2001 The influence of rays on the transverse elastic anisotropy in green wood of deciduous trees. *Holzforschung* **55**, 449 - 454.

Carlquist, S. 1988 *Comparative wood anatomy: systematic, ecological, and evolutionary aspects of dicotyledon wood*. Springer-Verlag, Berlin, 358 pp.

Clarke, S.H. 1933 On estimating the mechanical strength of the wood of ash (*Fraxinus excelsior* L.). *Forestry* **7**, 26 – 31.

Cote, W.A. and Hanna, R.B. 1983 Ultrasound characteristics of wood fracture surfaces. *Wood Fiber Sci.* **15**, 135 - 163.

Coureau, J.L., Morel, S. and Dourado, N. 2013 Cohesive zone model and quasibrittle failure of wood: a new light on the adapted specimen geometries for fracture tests. *Eng. Fract. Mech.* **109**, 328 - 340.

de Moura, M.F.S.F., Campilho, R.D.S.G. and Goncalves, J.P.M. 2008 Crack equivalent concept applied to the fracture characterization of bonded joints under pure mode I loading. *Compos. Sci. Technol.* **68**, 2224 - 2230.

Delorme, A. and Verhoff, S. 1976 Cell wall deformation in Norway spruce due to damage by storms, as revealed by scanning electron microscopy. *Holz als Roh- und Werkstoff* **33**, 456 - 460. Eng. Transl. OOENV TR-1146, Dept. Environ. Canada. 19 pp. 11 Refs.

Desch, H.E. and Dinwoodie, J.M. 1996 *Timber, structure, properties, conversion and use*. Macmillan Press, London, 306 pp.

Dinwoodie, J.M. 1981 *Timber: Its nature and behaviour.* New York: Van Nostrand Reinhold, 190 pp.

Easterling, K.E., Harrysson, R., Gibson, L.J. and Ashby, M.F. 1982 On the mechanics of balsa and other woods*. Proc. R. Soc. Lond. A* **383**, 31 - 41.

Ennos, A.R. 2001 *Trees*. The Natural History Museum, London, 112 pp.

Ennos, A.R. and van Casteren, A. 2010 Transverse stresses and modes of failure in tree branches and other beams. *Proc. Roy. Soc. Lond. B* **277**, 1253 – 1258.

Fruhmann, K., Reiterer, A., Tschegg, E.K. and Stanzl-Tschegg, S.S. 2002 Fracture characteristics of wood under mode I, mode II and mode III loading. *Philosophical Magazine A* **82**, 3289 – 3298.

Gartner B.L., Bullock S.H., Mooney H.A., Brown V.B. and Whitbeck J.L. 1990 Water transport properties of vine and tree stems in a tropical deciduous forest. *Am. J. Bot*. **77**, 742 – 749.

Gibson, L.J. 2005 Biomechanics of cellular solids. *J. Biomech*. **38**, 377 - 399.

Gibson, L.J. and Ashby, M.F., 1982 The mechanics of three-dimensional cellular materials. *Proc. Roy. Soc. Lond. A* **382**, 43 - 59.

Gibson, L.J., Ashby, M.F. and Easterling, K.E. 1988 Structure and mechanics of the iris leaf. *Journal of Materials Science* **23**, 3041 - 3048.

Gordon, J.E. and Jeronimidis, G. 1974 Work of fracture of natural cellulose. *Nature* **252**, 116 pp.

Gordon, J.E. and Jeronimidis, G. 1980 Composites with high work of fracture (and discussion*). Phil. Trans. R. Soc. Lond. A* **294**, 545 - 550.

Hardacker, K.W. and Brozinski, J.P. 1973 The individual fiber properties of commercial pulps. *TAPPI* **56**, 154 - 157.

Haygreen, J.G. and Bowyer, J.L. 1982 *Forest products and wood science: An introduction*. Iowa State University Press, 495 pp.

Ifju, G. and Kennedy, R.W. 1962 Some variables affecting microtensile strength of Douglas-fir. *Forest Products Journal* **12**, 213 - 217.

Jeronimidis, G. 1980 The fracture behaviour of wood and the relations between toughness and morphology. *Proc. R. Soc. Lond. B* **208**, 447 – 460.

Johnson, J.A. 1973 Crack initiation in wood plates. *J. Wood Sci.* **6**, 151 - 158.

Kahle, E.E. and Woodhouse, J.E. 1994 The influence of cell geometry on the elasticity of softwood. *Journal of Materials Science* **29**, 1250 - 1259.

Keith, C.T. and Cote, W.A. 1968 Microscopic characterization of slip lines and compression failures in wood cell walls. *Forest Products Journal* **18**, 67 - 74.

Kretschmann, D.E. and Green, D.W. 1996 Modelling moisture content-mechanical property relationships for clear Southern pine. *Wood Fiber Sci.* **28**, 320 - 337.

Larsen, H.J. and Gustafsson, P.J.H. 1990 The fracture energy of wood in tension perpendicular to the grain - results from a joint testing project. Paper CIB-W18A/23-19-2, *Proc. of CIB-W18A Meeting 23*, Lisbon, Portugal.

Logemann, M. and Schelling, W. 1992 The fracture toughness of spruce and the essential influences–investigations for mode I. *Holz als Roh - und Werkstoff* **50**, 47 - 52.

Matsumoto, N. and Nairn, J.A. 2012 Fracture toughness of wood and wood composites during crack propagation. *Wood Fiber Sci.* **44**, 121 - 133.

Mattheck, C. and Breloer, H. 1994 *The body language of trees: A handbook for failure analysis*. H.M. Stationary Office, London, 240 pp.

Mattheck, C. and Kubler, H. 1995 *Wood-the internal optimization of trees*. Springer-Verlag, Berlin Heidelberg New York, 129 pp.

McMahon, T. 1973 Size and shape in biology. *Science* **179**, 1201 – 1204.

Moden, C.S. and Berglund, L.A. 2008 Elastic deformation mechanisms of softwoods in radial tension – cell wall bending or stretching? *Holzforschung* **62**, 562 - 568.

Nairn, J.A. 2007 Material point method simulations of transverse fracture in wood with realistic morphologies. *Holzforschung* **61**, 375 - 381.

Niklas, K.J. 1992 *Plant biomechanics: An engineering approach to plant form and function*. University of Chicago Press, Chicago, 622 pp.

Ozden, S. and Ennos, A.R. 2014 Understanding the function of rays and wood density on transverse fracture behaviour of green wood in three species. *Journal of Agricultural Science and Technology B* **4**, 731 - 743.

Page, D.H., El-Hosseiny, F. and Winkler, K. 1971 Behaviour of single wood fibres under axial tensile strain. *Nature* **229**, 252 – 253.

Panshin, A.J. and de Zeeuw, C. 1980 *Textbook of wood technology-structure, identification, properties, and uses of the commercial woods of the United States and Canada*. 4th edn. McGraw-Hill Book Co., New York, 722 pp.

Persson, K. 2000 Micromechanical modelling of wood and fibre properties. *Doctoral Thesis*. Department of Mechanics and Materials, Lund University, Sweden.

Petterson, R.W. and Bodig, J. 1983 Prediction of fracture toughness in conifers. *Wood Fiber Sci.* **15**, 302 - 316.

Porter, A.W. 1964 On the mechanics of fracture in wood. *Forest Prod. J.* **14**, 325 - 331.

Price, A.T. 1929 A mathematical discussion on the structure of wood in relation to its elastic properties. *Phil. Trans. R. Soc. Lond. A* **228**, 1 - 62.

Reiterer, A., Burgert, I., Sinn, G. and Tschegg, S.E. 2002b The radial reinforcement of the wood structure and its implication on mechanical and fracture mechanical properties-a comparison between two tree species. *J. Mater. Sci.* **37**, 935 – 940.

Reiterer, A., Lichtenegger, H., Fratzl, P. and Stanzl-Tschegg, S.E. 2001 Deformation and energy absorption of wood cell walls with different nanostructure under tensile loading. *J. Mater. Sci.* **36**, 4681 - 4686.

Reiterer, A., Sinn, G. and Stanzl-Tschegg, S.E. 2002a Fracture characteristics of different wood species under mode I loading perpendicular to the grain. *Mat. Sci. Eng. A* **332**, 29 - 36.

Rug, W., Badstube, M. and Schone, W. 1990 Determination of the fracture energy of wood in tension perpendicular to the grain. Paper No. 23-19-1. Proceedings of the Meeting of International Council for Building Research Studies and Documentation Working Commission W18A-Timber Structures. University of Karlsruhe, Karlsruhe, Germany.

Schniewind, A.P. 1959 Transverse anisotropy of wood: A function of gross anatomic structure. *Forest Prod. J.* **9**, 350 - 359.

Schniewind, A.P. and Centeno, J.C. 1973 Fracture toughness and duration of load factor I. six principal systems of crack propagation and the duration factor for cracks propagating parallel to grain. *Wood Fiber Sci.* **5**, 152 – 159.

Simpson, W. and Anton, T. 1999 Physical properties and moisture relations of wood. Wood handbook: Wood as an engineering material. Madison, WI: USDA Forest Service, Forest Products Laboratory. General technical report FPL; GTR-113: Pages 3.1-3.24.

Smith, I. and Chui, Y.H. 1994 Factors affecting mode I fracture energy of plantation-grown red pine. *Wood Sci. Technol.* **28**, 147 - 157.

Stanzl-Tschegg, S.E., Tan, D.M. and Tschegg, E.K. 1995 New splitting method for wood fracture characterization. *Wood Sci. Technol.* **29**, 31 - 50.

Thomas, P. 2000 *Trees: Their natural history*. Cambridge University Press, Cambridge, 292 pp.

Tschegg, E.K., Reiterer, A., Pleschberger, T. and Stanzl-Tschegg, S.E. 2001 Mixed mode fracture energy of spruce wood. *J. Mater. Sci.* **36**, 3531 - 3537.

Tukiainen, P. and Koponen, S. 2006 Fracture behaviour of small wood specimens in RT direction. In: Proceedings of the 10th world conference on timber engineering. Portland, OR, USA, 55 pp.

Valentin, G.H., Bostrom, L., Gustafsson, P.J., Ranta-Maunus, A. and Gowda, S. 1991 *Application of fracture mechanics to timber structures, RILEM state-of-the-art report*. VTT Research Notes 1262. Technical Research Centre of Finland, Espoo, Finland, 142 pp.

van Casteren, A., Sellers, W.I., Thorpe, S.K.S., Coward, S., Crompton, R.H. and Ennos, A.R. 2012 Why don't branches snap? The mechanics of bending failure in three temperate angiosperm trees. *Trees – Structure and Function* **26**, 789 - 797.

Vasic, S. and Stanzl-Tschegg, S. 2007 Experimental and numerical investigation of wood fracture mechanisms at different humidity levels. *Holzforschung* **61**, 367 – 374.

Watanabe, U., Fujita, M. and Norimoto, M. 2002 Transverse Young's Moduli and cell shapes in coniferous earlywood. *Holzforschung* **56**, 1 - 6.